Hindawi
Advances in Materials Science and Engineering
Volume 2021, Article ID 4494056, 13 pages
https://doi.org/10.1155/2021/4494056

Research Article

Early Age Hydration Characteristics of Calcium Sulphoaluminate Cement Mortar Cured at a Temperature Range from −10 to 20°C

Zhongyu Chen,[1] Jianhong Fang,[2] Feng Ming,[3] and Yuhang Liu[3]

[1]*Qinghai Communications Holding Group Co. Ltd., Xining 810000, China*
[2]*Qinghai Research Institute of Transportation, Xining 810016, China*
[3]*State Key Laboratory of Frozen Soil Engineering, Northwest Institute of Eco-Environment and Resources, Chinese Academy of Sciences, Lanzhou 730000, China*

Correspondence should be addressed to Feng Ming; mf0329@163.com

Received 22 July 2021; Accepted 11 September 2021; Published 8 October 2021

Academic Editor: Rotana Hay

With the increasing number of infrastructures constructed in marine and cold regions, research on and applications of calcium sulphoaluminate (CSA) cement have been flourished, but the hydration process of CSA at low temperature has not been systematically investigated. To characterize the influence of low temperature on the hydration characteristics, freshly mixed CSA mortars were cured at −10, −5, 0, 5, and 20°C, respectively. The hydration process was investigated by electrical resistivity, compressive strength, and microstructure analyses. Results show that the hydration process (especially the induction period) is lengthened by low curing temperature. Both the electrical resistivity and compressive strength increase with an increase in the curing temperature. The compressive strength was reduced at a low curing temperature. Among these five curing temperatures, 5°C is the optimal curing temperature. Low temperatures do not change the kinds of hydrates, but reduce their amount. The scanning electron microscopy results illustrate that fewer hydrates fill the pores in specimens cured at low temperatures, while more hydrates form at higher temperatures. Moreover, low curing temperature contributes to the formation of coarse ettringite crystals. For the cement used at low temperature, the induction period should be reduced by adjusting the calcining process and composition proportion.

1. Introduction

Over nearly three decades, many infrastructures have been constructed in China, which has greatly promoted the development of concrete structures and cements [1]. The future development of cold and polar regions has become a trend. However, traditional Portland cement cannot meet the needs of engineering constructions in these low temperature areas, such as high-early strength and better expansion fill performance. Compared with other types of cement, calcium sulphoaluminate (CSA) cement has the advantages of fast setting, high early strength, and short construction period [2]. CSA cement is not only suitable for projects with high resistance to erosion, but is also very suitable for projects in cold regions. Moreover, CSA cement is one of the most economical rapid hardening cements with an annual output about approximately 1.3 million tons [3]. Motivated by the demand for environment protection and other special requirements, research on and applications of CSA have received increasing attention [4–6]. However, the hydration process of CSA at low temperatures is not well characterized.

To date, many methods have been used to quantify the hydration degree of cement [7–11]. During the hydration process, with the consumption of free water, the resistivity of mortar exhibits a large change. Therefore, the hydration process can be indirectly reflected by measuring its resistivity [12]. Moreover, resistivity can combine the chemical reaction with the changes in physical properties. Thus, it has been used to describe the hydration characteristics of cement at an early age [13]. Tamas noted out that two maxima appeared in the resistivity curves: the first one occurred at 1–3 hours, and the second one occurred at 6–10 hours [14]. Furthermore, the time of the first maxima is close to the initial setting time [15, 16]. Because the plasma impedance

can accurately reflect the variation in the ion concentration and structure [17], the electrical resistivity method has been adopted as a standard method in cement engineering [18]. Based on the electrical resistivity and its differential curves, the hydration process was first divided into three stages [12] and then four stages [19].

The hydration process is accompanied by the variation in the pore structure. The resistivity is an effective parameter for describing the formation of the pore structure [20]. It is found that the diffusion coefficient of ions in porous media has a proportional relationship to their resistivity, and that their permeabilities can be evaluated by their resistivities [21]. However, results have indicated that the diffusivity measured by the resistivity method is larger than that measured by other methods. Moreover, there is no significant association between the diffusivity and porosity when the admixtures are added [22]. As an improvement, on the basis of the Nernst–Einstein equation, the resistivity has been adopted as a rapid test method for determining the permeability of concrete. This method can be applied only when the pores are saturated with saltwater. Even so, this has not prevented the resistivity method from becoming the standard method for determining the permeability of concrete [23, 24]. Moreover, there is a quantitative relationship between the electrical resistivity and pore structure during the hydration process [20]. Because the porosity and pore structure are closely related to strength, the compressive strength can be predicted through resistivity [25, 26]. In addition, studies have demonstrated that resistivity can not only describe the evolution of the pore structure, but also can be used to evaluate the damage degree [27]. In other words, the resistivity is a key parameter for the evaluation of the pore structure and durability of concrete [28, 29].

Because ettringite (AFt)/monosulphoaluminate (AFm) has an obvious influence on compressive strength, many laboratory tests have been conducted to investigate the formation conditions of AFt/AFm. It is found that temperature has a great influence on the hydration process of cement paste. However, some researchers have found that the amount of AFt and AFm reaches the maximum at 20°C and 40°C [30], while some researchers have noted out that the stable product is AFt at 80°C, while AFm at 120°C, respectively [31]. Researchers believe that ettringite starts to dehydrate rapidly at approximately 50°C under normal humidity conditions [32]. These results indicate that an elevated temperature can accelerate the formation of AFm [33]. It can be seen that temperature not only influences the hydration process, but also influences the kinds of hydration products. At present, there are few studies on the hydration mechanism of CSA cement at low (subzero) temperatures. Furthermore, the influence of temperature on the hydration process is not uniform, which provides an opportunity to study the hydration mechanism of CSA cement cured at low (subzero) temperatures.

It can be concluded that the resistivity method has been widely used to characterize the hydration behavior of cement in the early stage. However, few studies have focused on the resistivity of CSA cement cured at low temperatures, especially at subzero temperatures. The lack of data on the CSA cement cured at low temperatures has hampered the further application of CSA cement in cold regions. Therefore, a series of macro- and microtests were conducted. In this study, the hydration characteristics at low temperatures were investigated, and the variations in resistivity, compressive strength, and hydration products were analyzed.

2. Materials and Methods

2.1. Raw Materials. A rapid hardening calcium sulphoaluminate cement, which was taken from Tangshan, China, was used in this study. Tables 1 and 2 show the chemical components and the physical properties of the CSA cement, respectively. Figure 1 presents the X-ray diffraction pattern.

A commercial standard sand was used, and its particle size distribution is shown in Table 3.

The antifreeze was ethanediol (C_2H_5OH, analytical pure, with a mass fraction greater than 99.7% and a density of 0.789~0.791 g/ml at 20°C), with a mass fraction of 10% of water (this content can keep the water from freezing at −10°C). Tap water was used to mix the mortar.

2.2. Specimen Preparation. According to the national standards (methods of testing cement-determination of strength (GB/T 17671)), the cement-sand ratio was determined as 1 : 3. Two water-cement ratios (w/c = 0.4 : 1 and w/c = 0.5 : 1) were adopted in the laboratory tests. The raw material was stirred uniformly by a planetary-type mixer. First, the cement, ethanediol, and water were mixed for 30 s at 60 rpm. Second, sand was added and mixed for 30 s at 60 rpm. Third, mixing was stopped 90 s and further mixing was continued for 90 s at 120 rpm. Then, the mortars were ready for electrical resistivity and compressive strength tests. These sample preparation steps were conducted at room temperature (approximately 25°C).

2.3. Curing Conditions. A thermostat (temperature range −30~60°C with an accuracy of 0.1°C) was used to provide the required temperature. Before the electrical resistivity test, the thermostat's temperature was set at the required value for at least 12 hours. Later, specimens were placed into the thermostat, and the temperature remained unchanged until the resistivity test was completed. The specimens were wrapped with plastic bag, so they were cured under airtight conditions.

2.4. Testing Procedure. The samples were only prepared for electrical resistivity and compressive strength tests. The samples used for scanning electron microscopy (SEM), X-ray diffraction (XRD), and Mercury intrusion porosimetry (MIP) tests were selected from the crushed samples (after the compressive strength test). The flow chart is shown in Figure 2.

2.4.1. Electrical Resistivity. The electrical resistivity test methods included two phase electrodes, four phase electrodes, and noncontact test techniques. Here, to reduce the

Table 1: Chemical components of the CSA cement (wt/%).

Material	Al_2O_3	CaO	SiO_2	SO_3	Fe_2O_3	MgO	TiO_2	LOI
CSA cement	33.36	43.01	8.28	7.90	1.95	1.69	1.35	0.89

Table 2: Physical properties of the CSA cement.

Material	Specific surface area (m^2/kg)	Density (kg/m^3)	Setting time (min)	
			Initial setting	Final setting
CSA cement	460	2900	26	43

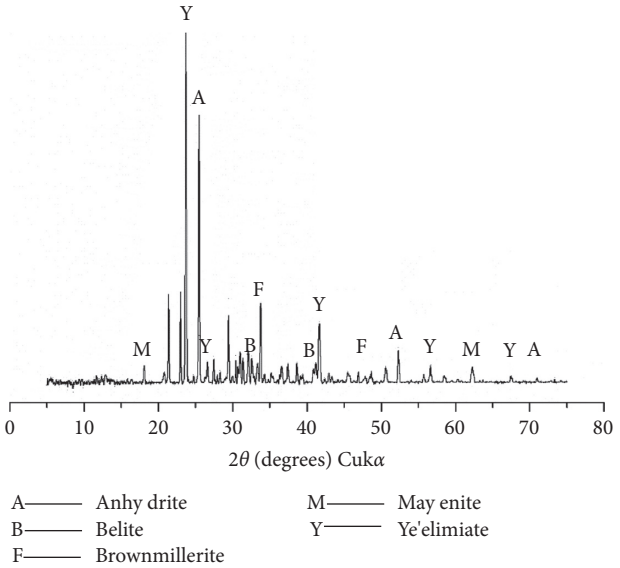

Figure 1: X-ray diffraction pattern of the tested cement.

Table 3: Particle size distribution of the sand.

Size (mm)	2.0	1.6	1.0	0.5	0.16	0.08
Accumulated retained (%)	0	7 ± 3	32 ± 3	65 ± 3	87 ± 3	99 ± 1

disturbance caused by the electrodes, the two phase electrode method was used in the resistivity test. A content of 500 g of mortar was placed into a plastic bucket (with a diameter of 65 mm and the length was measured after the test), and, then, one copper plate was fixed at each sidewall of the specimen. The copper plates and the resistivity testing equipment (type: TH 2830) were connected by a conducting wire. After sample preparation, the specimens for the resistivity test were placed into the thermostat. The resistance was automatically recorded by TH 2830 resistivity testing equipment at an interval of 5 min. The testing frequency is 10 kHz. The schematic diagram of the resistivity test is shown in Figure 3. The resistivity can be calculated as follows:

$$\rho = R\frac{A}{L}, \quad (1)$$

where ρ is the resistivity, R is the resistance, A and L are the area and length of the sample, respectively.

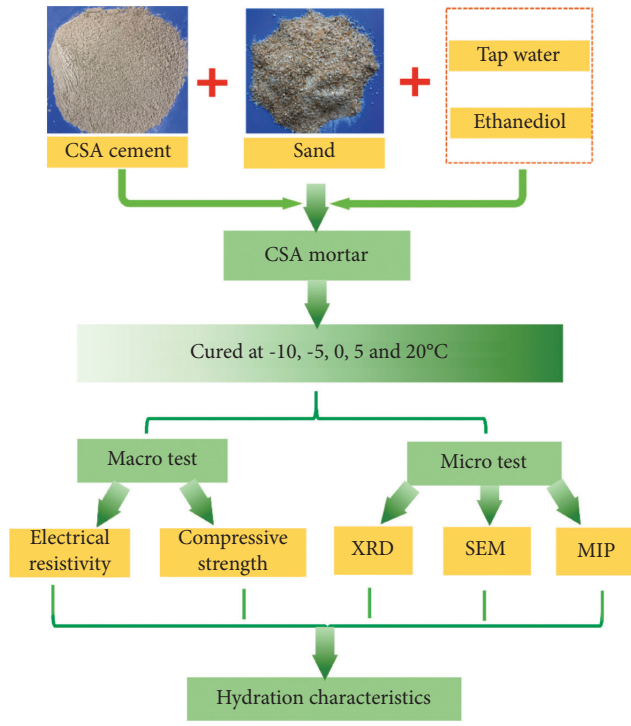

Figure 2: Flow chart of the laboratory tests.

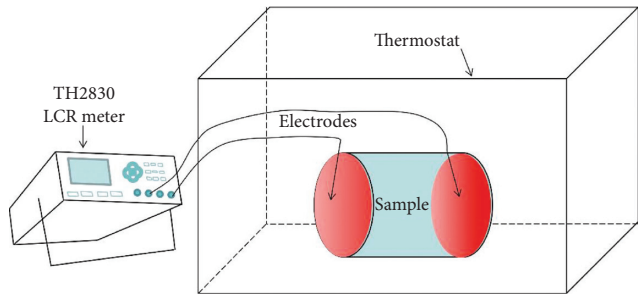

Figure 3: Schematic diagram of the electrical resistivity test at different temperatures.

2.4.2. Compressive Strength Tests. The mortar was poured in a steel mold (with a size of 40 mm × 40 mm × 40 mm), and the mold was vibrated. Then, the mold was wrapped in a plastic bag. Finally, the specimens were cured at constant temperatures of −10, −5, 0, 5, and 20°C for 24 hours, and then demolded and kept at the required temperature. The compressive strength tests were carried out at days 1, 3, and 7 on a universal testing machine with a loading rate of 2.4 kN/

s. The average value of the three specimens was used to determine the compressive strength. If the range was more than 30% of the average value, the value with the largest deviation was eliminated, and the average of the other two values was taken as the compressive strength.

2.4.3. SEM, XRD, and MIP Tests. After the compressive strength, the crushed specimens with a size of 10–20 mm were selected and immersed in ethyl alcohol for 7 d to stop hydration and then dehydrated in a drying oven at 45°C for 24 hours. After that, the specimens were crushed again, and the specimens with a size of 5–10 mm were selected. A fresh fractured surface was scanned by using the field emission scanning electron microscope (ESEM, QUANTA FEG 450). Phase analysis was conducted by using X-ray diffraction (type: Bruker D8A). The diffraction patterns were recorded within 10°–75° (2θ) with 0.01°/step. Finally, the pore structure characteristics were investigated by using the MIP tests (type: Autopore IV 9500).

3. Results

3.1. Electrical Resistivity. Figure 4 presents the development of the electrical resistivity of the mortars cured at different temperatures. The laboratory results indicate that the resistivity of mortar increases with curing time. The resistivity method actually tests ion migration in cementitious materials [11]. After water was added to the cement, the amount of ions released by the cement particles in the liquid phase continuously changed. In the dissolution and induction stages, less water and ions were consumed, and there was little change in the resistivity. At the acceleration stage, the fast consumption of ions and water led to the formation of a large amount of hydrates and gradually reduce the liquid phase space. This results in poor water connection. Therefore, the resistivity gradually increased [19]. However, there is the same difference between the results of two water-cement ratios. As presented in Figure 4(a), at the same cured age and temperature, the samples with low water-cement ratio (0.4) have a larger resistivity than the samples with a high water-cement ratio (0.5).

CSA cement is a rapid hardening cement, it enters the acceleration stage quickly at 20°C, and thus the resistivity rapidly increases from 2 hours [11]. However, low temperatures delay the hydration process. As shown in Figure 4(b), the electrical resistivity is relatively large at 30 hours when the samples are cured at 5 and 20°C. The electrical resistivity is relatively small before 60 hours when the samples are cured at −10 and −5°C. Compared with the samples cured at a low temperature, the samples cured at a high temperature have larger changes in the resistivity rate, no matter the water-cement ratio. Moreover, when the curing temperature is above 5°C, the resistivity curves have a consistent trend and include four parts: a slight increase, a decrease, stabilization, and then an increase followed by a gradual stabilization. With the decreasing curing temperature (at −10°C), the stabilization part does not appear on the resistivity curve. It is evident that the acceleration stage appears significantly earlier with an increasing curing temperature, and this indicates that a lower temperature lengthens the induction stage and delays the hydration process.

Previous studies have indicated that ions released by cement cause a decrease in electrical resistivity [11, 16]. As shown in Figures 4 and 5, there is a slight increase in electrical resistivity and the increment increases gradually with the decrease in the curing temperature. There are two reasons for the change in resistivity in the dissolution stage. One reason is the temperature decrease (from room temperature 25°C to the tested temperature), and the other reason is the dissolution of soluble ions from cement particles. The former increases resistivity, and the later decreases resistivity. The diminution of resistivity is not apparent, and resistivity shows an increasing trend. The result shows little difference from the results presented by literature [11]. This can be explained by the fact that (1) low temperatures impede the dissolution of ions and (2) the decrease in resistivity has little change (less than 0.5 Ω m) [11, 16]. Furthermore, the hydration process gradually reaches the acceleration stage. However, the hydration process is significantly delayed by the low curing temperature (−10°C and −5°C). As seen in Figures 5(a) and 5(b), the curves of variation rate of resistivity have similar change trends: there are two peaks in the curves of the variation rate of resistivity when the samples are cured at 20°C, 5°C, and 0°C. Only one peak is observed at −5°C and −10°C. However, the node time is different for different water-cement ratios. For the sample with low water-cement ratio cured at 0°C and 5°C, the acceleration stages start from 30 hours to 8.6 hours, respectively (Figure 5(a)). For the sample with high water-cement ratio cured at 0°C and 5°C, the acceleration stages start from 15.7 hours to 7.5 hours, respectively (Figure 5(b)). As shown in Figure 4, the horizontal segment (induction stage) is extended with the decreasing temperature, especially at −10°C and −5°C. In the acceleration stage, the hydrates are continuously formed [34]. The length of the conducting path increased, which caused the increase in resistivity. In addition, the rate of electrical resistivity decreases with decreasing curing temperature, which can be explained by the fact that a higher temperature can improve the activity of the raw materials and promote the hydration process.

3.2. Compressive Strength. The compressive strength of CSA mortars cured at different temperatures was measured in 1 d, 3 d, and 7 d. The compressive strength of CSA mortar increases with increasing curing age, regardless of the curing temperature and water-cement ratio. As shown in Figure 6(a), the compressive strength of the sample cured at −10°C is about 3.23 MPa at day 1, which is only approximately 10% of that of the specimens cured at 20°C (28.83 MPa). The similar result can be found in Figure 6(b). The test results indicate that the compressive strength decreases sharply at low curing temperature, especially from 0 to 1 d. Although the low temperature slows the hydration rate, the compressive strength continuously increases with the curing time. Moreover, at a water-cement ratio of 0.5, the

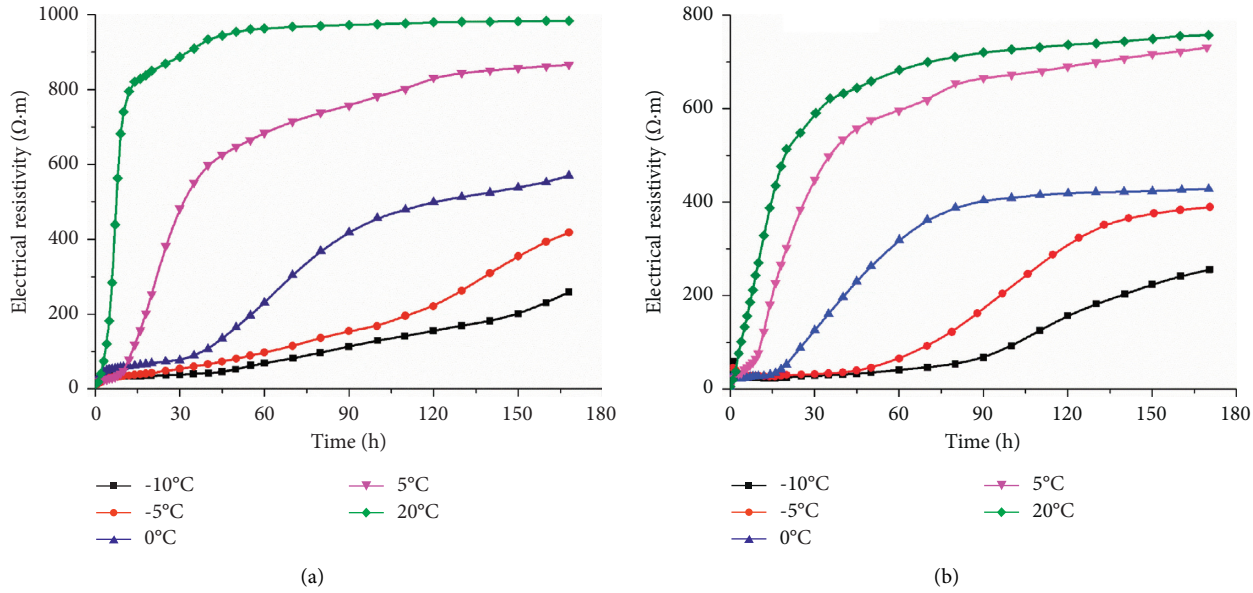

Figure 4: Electrical resistivity of the mortar at different curing temperatures during 0–7 d. (a) w/c = 0.4; (b) w/c = 0.5.

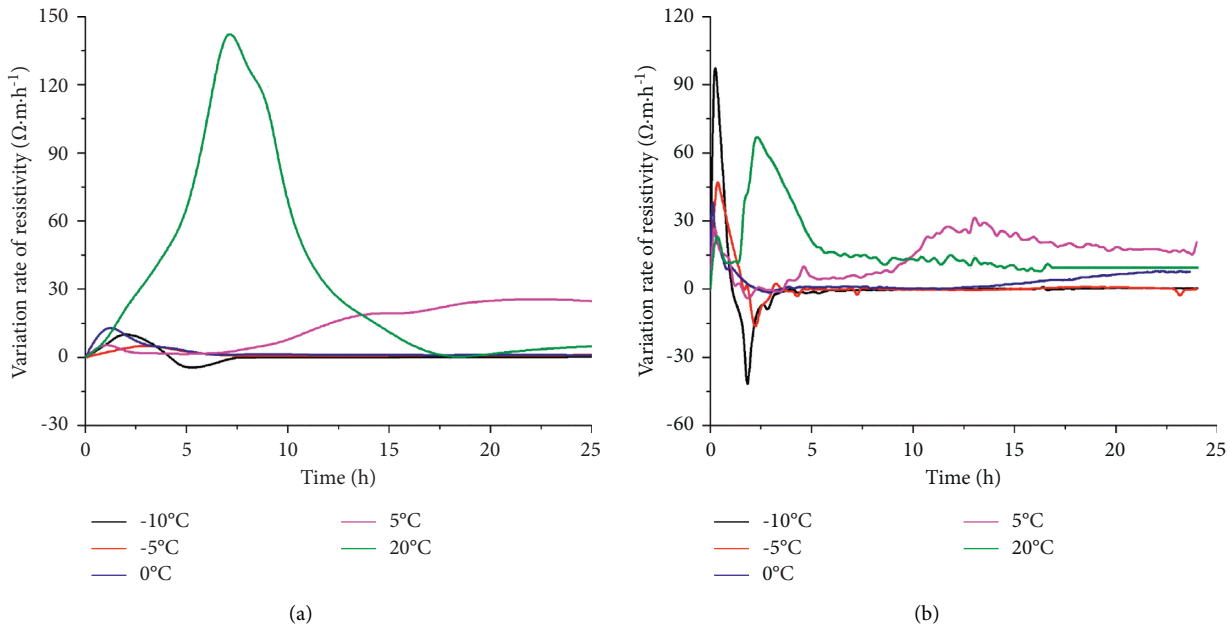

Figure 5: Rate of electrical resistivity of the mortar at different curing temperatures for 0–1 d. (a) w/c = 0.4. (b) w/c = 0.5.

compressive strength of the specimen cured at −5°C for 7 d is only approximately 2 MPa lower than that of the sample cured at 0°C. The sample cured at 5°C has a compressive strength of 46.4 MPa, while the sample cured at 20°C has a compressive strength of 43.6 MPa. This trend is similar to the results presented by Xu et al. [33]. It can be concluded that there is an optimal curing temperature for CSA cement cured at temperatures ranging from −10°C to 20°C.

As shown in Figure 6, at these two water-cement ratios, the early strength of the mortars decreased significantly at low curing temperature. This is because a lower curing temperature delays the hydration process and decreases the hydration rate, which leads to a decrease in the amount of hydrates. It is known that the strength of the CSA mortar is controlled by the amount of AFt crystals and its microstructure. When samples have the same hydration degree, the connection between the hydration products and the microstructure controls the strength [35]. As mentioned above, a low curing temperature slows the hydration rate. Therefore, the sample cured at a lower temperature has a lower hydration degree than that cured at a high temperature [36]. In other words, a lower curing temperature decreases the hydration degree and reduces the amount of hydrates. Consequently, an unstable microstructure is

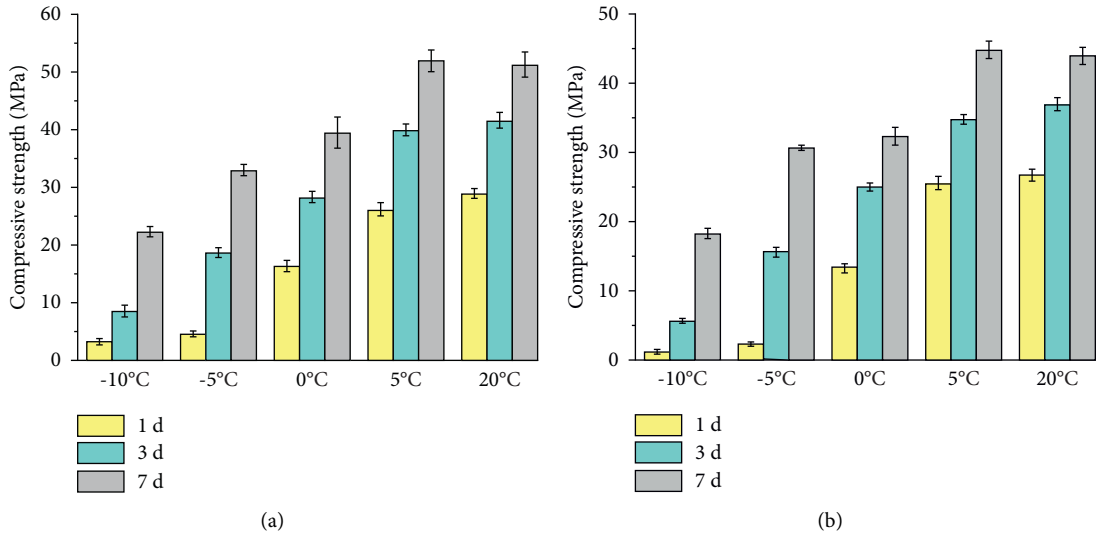

Figure 6: Compressive strength of mortar cured at −10, −5, 0, 5, and 20°C. (a) w/c = 0.4. (b) w/c = 0.5.

formed in the mortars without the connection provided by the hydration production. Therefore, the compressive strength decreases at low curing temperatures, no matter the water-cement ratio.

3.3. X-Ray Diffraction (XRD). Figure 7 shows the XRD patterns of CSA mortars cured under different conditions. Previous study indicates that the main hydration products of CSA cement are ettringite (AFt), monosulphoaluminate (AFm), and alumina gel (AH_3) [3]. This can be verified by the microanalysis (Figures 7 and 8). However, the main hydration product of the samples cured at −10, −5, and 0°C is AFt, almost without AFm and AH_3 (Figure 8). For the sample cured at 5 and 20°C, the dominant hydrates are AH_3 and AFm. This can be explain the fact that the formation of hydrates is determined by the hydration degree, as reflected by the consumption of gypsum. When calcium sulfate is completely consumed, hydrates of AFm and AH3 will gradually form according to (2) [3]. As noted by Wang et al., the AFm will form in the middle of the hydration process. The XRD results show that the specimens cured at 20°C have early access to the middle of the hydration process, which illustrates that the hydration process is delayed by low curing temperature [35].

$$C_4A_3S + 18H_2O \longrightarrow C_4ASH_{12}\,(\text{AFm}) + 2AH_3 \qquad (2)$$

As shown in Figure 7(b), with prolonged hydration time, the diffraction peak of AFt increases gradually and the diffraction peak of Ye'eliminate decreases. In addition, because the hydration product AH_3 has poor crystallinity, it is difficult to characterize AH_3 by using XRD. From the details mentioned above, we can conclude that a low curing temperature only suppresses the hydration reaction and does not change the kinds of hydrates, but the amount of hydrates obviously decreases. Moreover, because the lower curing temperature delays the hydration process, the appearance time of AH_3 is postponed.

3.4. Scanning Electron Microscope (SEM). Figure 8 shows the microstructure of a hydrated paste cured at different temperatures for 3 d. For the sample cured at 20°C, the hydration products contain more plate-shaped AFm and pompon-shaped AH_3, almost without AFt (Figure 8(a)). With the decrease in curing temperature, small, short, and fine needle AFt gradually appears. At −10°C, more acicular ettringite can be observed in the specimens. In total, as the curing temperature drops from 20°C to −10°C, the AFm and AH_3 gradually disappear, and the AFt becomes coarser (Figure 8(e)). This finding can be explained by the fact that the solubility of ettringite at 20°C is larger than that at −10°C, so it is easy to form ettringite at low temperature [37]. In addition, the formation of hydrated calcium silicate gel at −10°C is slower than that at 20°C, and there is a large residual space between particles, which promotes the growth of ettringite [35]. Moreover, when gypsum is completely consumed, AFm will form according to equation (3) [3]. Therefore, the content of AFt at −10°C is higher than that at 20°C. In addition, a higher curing temperature results in faster conversion from AFt to AFm,

$$C_6AS_3H_{32}\,(\text{AFt}) + 2C_3A + 4H_2O \longrightarrow 3C_4ASH_{12}\,(\text{AFm}) \qquad (3)$$

As shown in Figure 8, with the elevated curing temperature, the amount of AH_3 gradually increases. Combined with the compressive strength results, it is found that the compressive strength increases with increasing curing temperature. This conclusion agrees well with the previous results [38]. During the hydration process, AFt forms first, but its structure is relatively loose and the compressive strength is low. By increasing the hydration time, the hydration degree increases and AH_3 is formed. Because AH_3 has a high cohesion and large specific surface area of approximately 285 m^2/g [39], the connection between components strengthened by AH_3. Moreover, as the AH_3 phase fills the pore spaces, the structure becomes relatively dense.

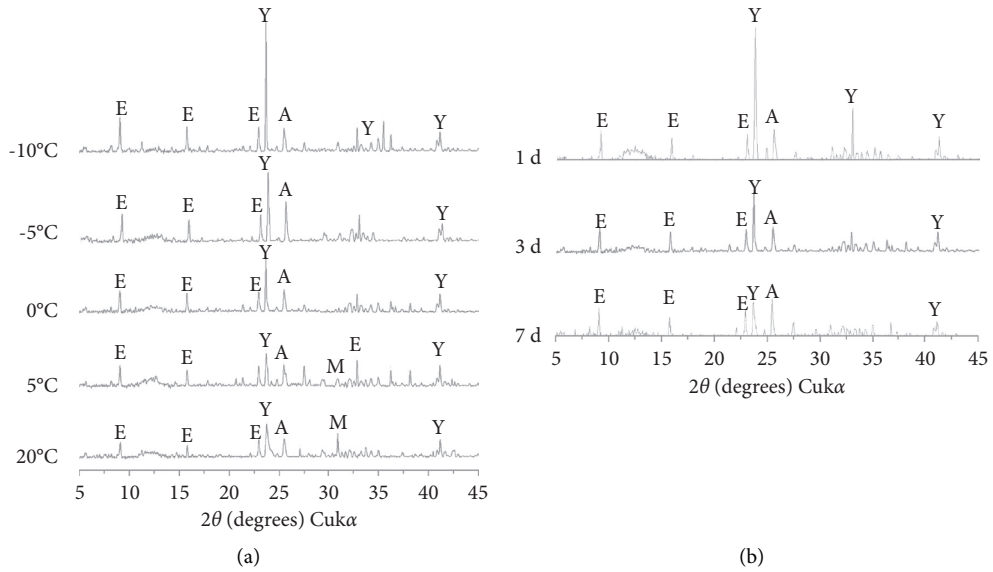

Figure 7: XRD patterns of mortars (E: ettringite, M: monosulphoaluminate, Y: Ye'eliminate, and A: anhydrite). (a) Samples cured at −10°C, −5°C, 0°C, 5°C, and 20°C for 3 d. (b) Samples cured at 0°C for 1 d, 3 d, and 7 d.

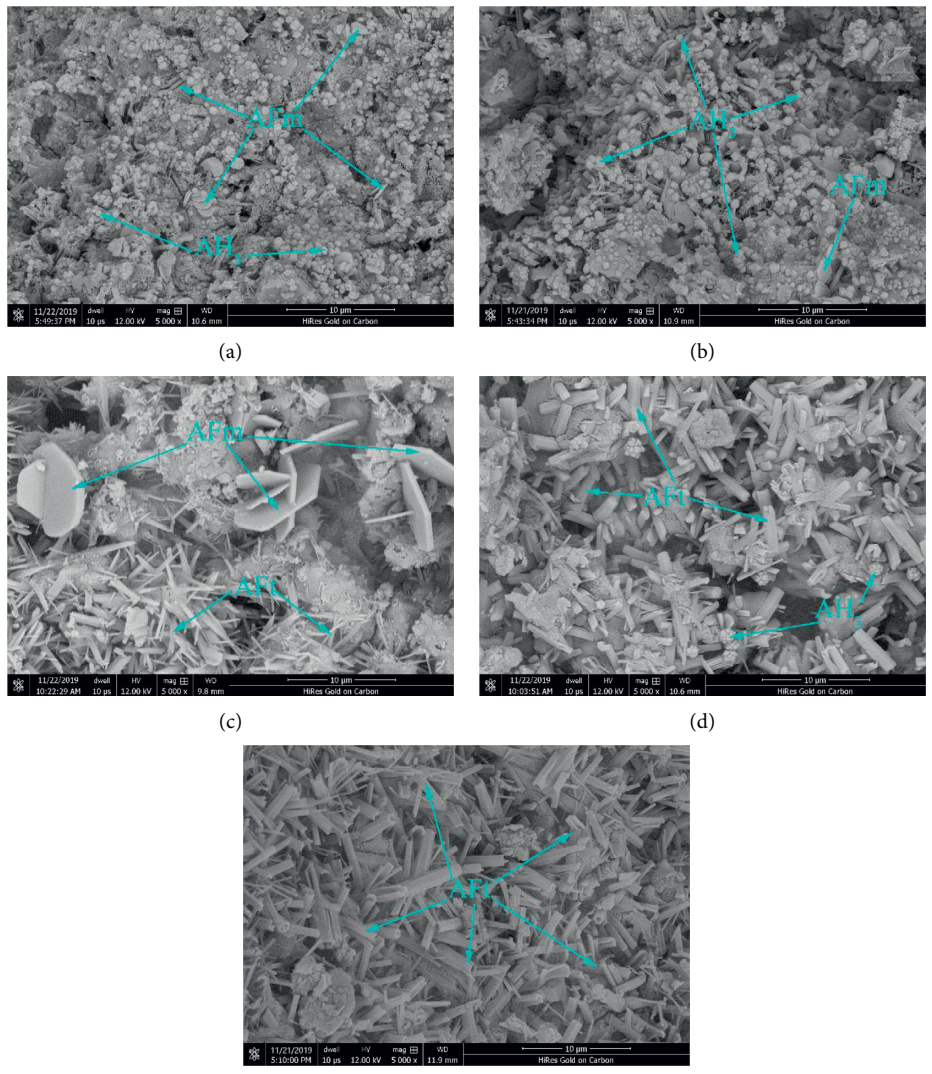

Figure 8: SEM images of CSA cement mortars cured at different curing temperatures for 3 d. (a) 20°C; (b) 5°C; (c) 0°C; (d) −5°C; (e) −10°C.

Therefore, the compressive strength increases with hydration time, and the elevated curing temperature can enhance the compressive strength.

3.5. Pore Sizes. The pore structure can be treated as one of the external manifestations of cement hydration. Figure 9 shows the pore size distribution of the specimens cured at different temperatures (w/c = 0.5). At day 3, the pore volumes of the samples cured at −10, −5, 0, 5, and 20°C are 0.288, 0.229, 0.213, 0.178, and 0.182 mL/g, respectively. The porosity results show that the curing temperature has a noticeable effect on the total porosity, and that 5°C is the optimum curing temperature to obtain a minimum porosity. Li et al. [40] pointed out that increasing the amount of hydration products will decrease the total porosity. As the temperature decreases, the hydration process is delayed. Consequently, the amount of the hydration product is reduced. Therefore, with less hydrates filling the pore space, porosity increases with the decreasing curing temperature. Moreover, the results show that the pore size distribution shows little difference at different curing temperatures. As shown in Figure 9, the volume of a pore with a diameter larger than 0.1 μm is 0.098 mL/g at −10°C and 0.031 mL/g at 20°C. Compared with the sample cured at 20°C, the number of coarse pores noticeably increases when the sample is cured at −10°C. The change law is consistent with the influence of high-temperature curing on the pore structure of the silicate cement [41, 42].

Because pores with different sizes have different effects on the physical-mechanical properties of concrete, the pores are divided into four classes depending on the endanger degree (Table 4) [43]. Total porosity varies little at 5°C and 20°C. However, the proportion of harmful pores is larger at 20°C than that at 5°C. As a result, the specimen cured at 5°C has a large compressive strength. This indicates that the optimal curing temperature can reduce the number of harmful pores.

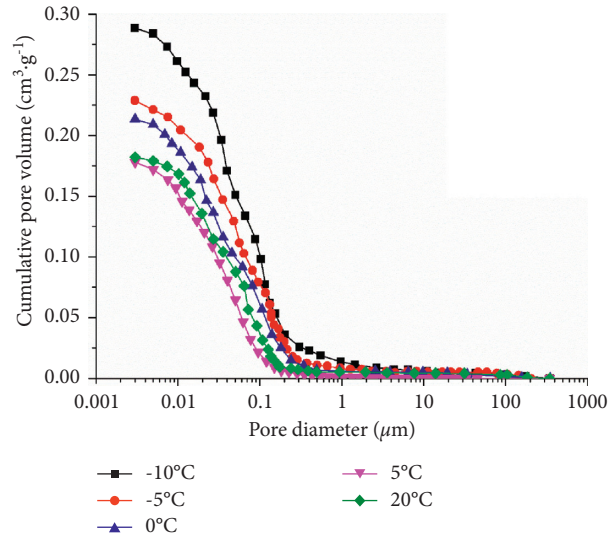

Figure 9: Pore structure of the CSA mortar at different curing temperatures for 3 d.

Table 4: Pore-class classification [43].

Pore size/nm	<20	20–100	100–200	>200
Hazard ranking	Harmless	Less harmful	Harmful	More harmful

4. Discussion

4.1. Influence of Temperature on the Formation of Strength. The experimental results indicate that an elevated temperature results in the compressive strength first increasing (cured at −10°C~5°C) and then decreasing (cured at 5°C~20°C). This changing trend does not completely agree with the results presented by Li et al., which showed that the strength tends to decrease with increasing curing temperature (samples were cured at 5°C~40°C) [40]. It is well known that concrete has a resistant freezing critical strength [44]. The compressive strength of the specimens cured at −10°C and −5°C for 1 d is lower than the resistant freezing critical strength of 2.5 MPa (the resistant freezing critical strength is determined by the literature [45]). Therefore, frost heaving stress, induced by pore water migration and freezing, will destroy the structure of the mortars cured at −10°C and −5°C and lead to a decrease in strength. Moreover, the specimens cured at −5°C and −10°C are still in the deceleration stage at day 7. This means that fewer hydrates form and the components in the mortar have a poor connection, which does not benefit in developing strength. For curing temperature over 5°C, there is no frost heaving stress. Under this condition, low temperatures are beneficial to the formation of ettringite and increase in strength [35]. Moreover, the specimens cured at 20°C and 5°C have reached the stable stage in 7 d. Many hydrates are formed, and the components are strengthened by the hydrates. Consequently, the mortar has a denser structure and a larger compressive strength. At a high temperature (20°C), due to the large hydration rate, more harmful pores will be formed. Results show that higher and lower curing temperatures result in an increase in the number of harmful pores. Thus, there is a critical curing temperature for obtaining the largest compressive strength and lowest porosity. Moreover, as shown in Table 5, the low temperature increases the total porosity and results in a decrease in the proportion of harmless pores.

4.2. Influence of Temperature on Electrical Resistivity. Previous results indicated that the liquid phase played a key role in determining the electrical resistivity [46]. After the mortar was mixed, the hardening of mortar occurs in three states: flow state, plastic state, and solid state. At the early time, both the ion concentration and the volume of the liquid phase were large. Sands are surrounded by pore water in the mortar. All the pores were connected with each other, and the length of the conducting path was short (Figure 10(a)). Consequently, the electrical resistivity was small. Due to the formation of hydration products, the porosity and free water content were reduced continually.

Table 5: Proportions of hazard ranking of pores.

Test condition	Hazard ranking				
	Harmless (%)	Less harmful (%)	Harmful (%)	More harmful (%)	Porosity (mL/g)
5°C, w/c = 0.4	51.28	21.60	8.38	18.74	0.110
5°C, w/c = 0.5	32.45	54.37	10.36	2.83	0.178
−5°C, w/c = 0.4	39.37	27.70	10.22	22.71	0.163
−5°C, w/c = 0.5	22.23	43.16	21.43	13.17	0.229

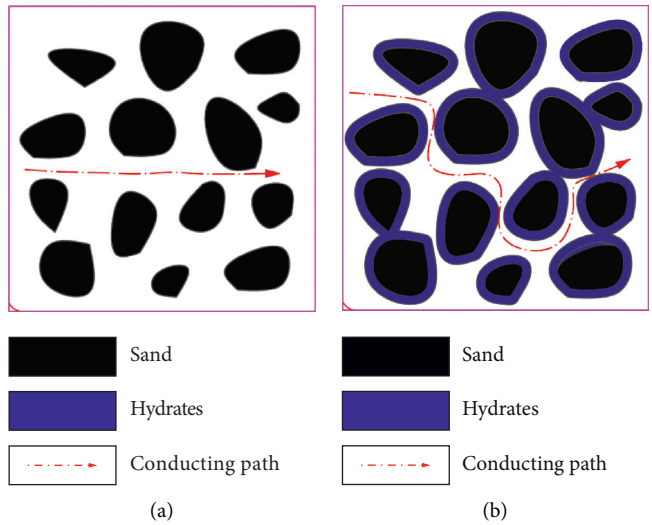

Figure 10: Schematic presentation of the conduction paths in the mortar (a) fresh mortar and (b) mortar hydrated for some time.

With time going on, the volume of the solid phase increases and the volume of the liquid phase decreases. Consequently, the hydration products broke the conduction path and lengthened the conducting path (Figure 10(b)). Moreover, the formation of hydrates consumed many ions. The decrease in ion concentration and the increase in the length of the conducting path led to a dramatic increase in resistivity.

Actually, the variation in electrical resistivity reflects the evolution of the pore structure. Here, the formation factor was used for describing the pore structure, which can be calculated as follows [24]:

$$F = \frac{\rho}{\rho_0}, \tag{4}$$

where ρ is the resistivity of the mortar and ρ_0 is the resistivity of the pore water in the mortar. All the ions were dissolved in water in the induction stage, and the minimum electrical resistivity was treated as ρ_0.

Based on the tested resistivity, the formation factor can be calculated, as shown in Figure 11. The results indicate that at these two water-cement ratios, the formation factor increases with prolonged hydration time. Moreover, as seen in Figure 6, at the same curing age and temperature, the sample with a low water-cement ratio has a larger electrical resistivity. With the hydration process going on, free water is gradually consumed and more hydrated cement is generated. This results in a decrease in the volume of the liquid phase and an increase in the volume of the solid phase [13]. As a result, the resistivity increases. Therefore, the formation factors increase with hydration time. Moreover, at the same age, specimens cured at high temperatures have a larger formation factor. This can be explained that a higher hydration degree indicates more free water and ions have been consumed. Therefore, compared with the specimens cured at lower temperatures, the sample cured at 20°C has the minimal volume for the liquid phase. A poor connection between pore water results in the longest conducting path formed in the sample cured at 20°C. Consequently, this sample has the largest resistivity and formation factor. Because the hydration rate is decelerated by low temperature, more free water exists in the pores, resulting in an increase in the volume of the liquid phase. Better pore water connection causes the decrease in resistivity. To some degree, the change in the formation factor can reflect the hydration degree. In addition, the sample with low water-cement ratio has a smaller change rate in the formation factor. A low water-cement ratio means that less water is added in the cement, and the pore water connection is poor, so the minimum electrical resistivity is larger in the low water-cement ratio. When the resistivity of the mortar has little difference, the formation factor was determined by the minimum electrical resistivity ρ_0.

4.3. Influencing Mechanism of Temperature on the Hydration Process. The hydration process can be summarized in three steps: dissolution of cement particles, consumption of free water, and formation of hydration products [3]. As seen, the low curing temperature did not change the final hydration products [47], but lengthened the hydration process (Table 6).

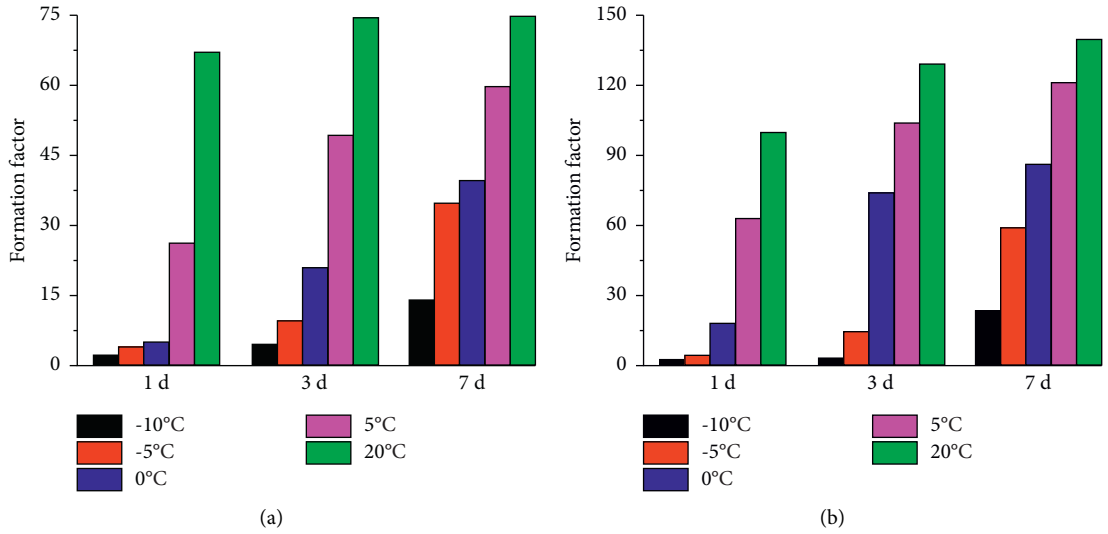

Figure 11: Variation in the formation factor at different curing temperatures for 1 d, 3 d, and 7 d. (a) w/c = 0.4; (b) w/c = 0.5.

Table 6: The initial time of the mortar access to different hydration stages (unit: hour).

Hydration stages	Curing temperature				
	20°C	5°C	0°C	−5°C	−10°C
Dissolution stage	0.0	0.0	0.0	0.0	0.0
Induction stage	0.8	2.4	3.5	4.2	4.8
Acceleration stage	1.4	7.5	15.7	28.6	80.2
Deceleration stage	2.5	12.5	24.5	77.4	118.1
Stabilization stage	16.2	48.4	101.3	—	—

Notes: The symbol "—" means does not appear. Water-cement ratio is 0.5.

Taking the age of 1 d, for example, the specimens with a water-cement ratio 0.5 cured at 20°C and 5°C have access to the deceleration stage, the specimens cured at 0°C have access to the acceleration stage, but the specimens cured at −5°C and −10°C are still in the induction stage. Moreover, the specimens cured at −5°C and −10°C still did not enter the stable stage even at 7 d.

The results indicate that the hydration process was lengthened by the low temperature. The key piece of evidence is that both compressive strength and electrical resistivity decreased with decreased curing temperature at the same age. Therefore, in some degree, we can conclude that the low curing temperature decreases the hydration rate. In this section, we will discuss how the temperature decreases the hydration rate.

The hardening of cement is accompanied by chemical reactions. Therefore, we will analyze the influencing mechanism from the perspective of chemical reactions. The "collision theory" in chemical reaction indicates that a reaction may occur when reactant molecules collide with each other [48, 49]. However, not every collision can result in a reaction, and only an "effective collision" can result in a reaction. An effective collision must meet two basic conditions: (1) the molecules have high energy and (2) the molecules collide with each other in a certain direction [49]. The collision theory also noted that both increasing the number of activation molecules and increasing the effective collision times can speed up the reaction rate. At a lower temperature, the molecules have lower energy and may not meet the required activation energy compared to that at a higher temperature, which means that a lower temperature will reduce the number of activation molecules (Figure 12(a)). Meanwhile, water is sticky at low temperatures, and ions encounter more resistance during the moving process. Therefore, the effective collision frequency is reduced by lower temperature (Figure 12(b)). As a result, the decrease in the number of activation molecules and the decrease in the effective collision frequency lead to a decrease in the hydration rate (Figure 12(c)). Thus, at the same age, the specimens cured at high temperature have a high hydration degree. In other words, the hydration process is lengthened by a lower curing temperature, as listed in Table 4. Moreover, the Arrhenius theorem indicates that the constant of the reaction rate decreases with decreasing temperature. Because the hydration process is suppressed by the low temperature, the amount of hydration products is reduced. In turn, the compressive strength decreases. In short, the low temperature decreases the hydration rate. Therefore, when designing the cement for low temperature, the induction period should be reduced.

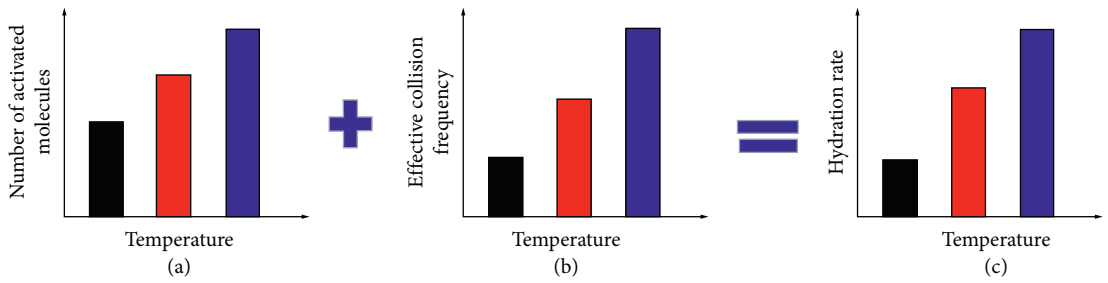

Figure 12: Schematic of the function of temperature on the hydration of CSA cement. (a) The elevated temperature can increase the number of activated molecules; (b) the elevated temperature can enhance the effective collision frequency, (c) With the increase in the number of activated molecules and the effective collision frequency, the hydration rate is accelerated by the elevated temperature.

5. Conclusion

A series of laboratory tests were conducted to investigate the influence of low temperatures on the hydration characteristics of CSA cement. Through systematic analyses, the following conclusions can be obtained:

(1) Temperature has a significant effect on the macroproperties of mortar. The influence degree of the temperature decreases with the increase in curing time. The hydration rate determines the early strength, but the later strength is controlled by the amount of hydrates and the microstructure.

(2) Low curing temperatures slows the hydration rate, lengthens the hydration process, and delays the transformation of AFt to AFm. The types of hydration products are not changed by low curing temperature, but their quantity decreases sharply with decreasing temperature, especially at the early stage.

(3) For the tested CSA cement, the optimum curing temperature is around 5°C. An appropriate hydration rate can decrease the number of harmful pores and increase the compressive strength. Therefore, in the engineering application, an appropriate curing temperature should be provided.

Data Availability

The datasets generated during and/or analyzed during the current study are available from the corresponding author on reasonable request.

Conflicts of Interest

The authors declare that they have no conflicts of interest.

Acknowledgments

This work was supported by the Basic Research Projects of Qinghai (grant number 2021-ZJ-908).

References

[1] W. Wang, "Analysis of the state of Chinese NSP cement industry technology development and reflection on its future," *Cement Engineering*, vol. 5, pp. 17–21, 2003.

[2] J. Péra and J. Ambroise, "New applications of calcium sulfoaluminate cement," *Cement and Concrete Research*, vol. 34, no. 4, pp. 671–676, 2004.

[3] Y. M. Wang, M. Z. Su, and L. Zhang, *Sulphoaluminate Cement*, Beijing University of Technology Press, Beijing, China, 1999.

[4] Z. He, H. Yang, and M. Liu, "Hydration mechanism of sulphoaluminate cement," *Journal of Wuhan University of Technology-Materials Science Edition*, vol. 29, no. 1, pp. 70–74, 2014.

[5] L. Coppola, D. Coffetti, E. Crotti, and T. Pastore, "CSA-based Portland-free binders to manufacture sustainable concretes for jointless slabs on ground," *Construction and Building Materials*, vol. 187, pp. 691–698, 2018.

[6] C. Liu, J. Luo, Q. Li et al., "Calcination of green high-belite sulphoaluminate cement (GHSC) and performance optimizations of GHSC-based foamed concrete," *Materials and Design*, vol. 182, Article ID 107986, 2019.

[7] J.-B. Champenois, C. Cau Dit Coumes, A. Poulesquen, P. Lc Bescop, and D. Damidot, "Beneficial use of a cell coupling rheometry, conductimetry, and calorimetry to investigate the early age hydration of calcium sulfoaluminate cement," *Rheologica Acta*, vol. 52, no. 2, pp. 177–187, 2013.

[8] D. Gastaldi, F. Canonico, and E. Boccaleri, "Ettringite and calcium sulfoaluminate cement: investigation of water content by near-infrared spectroscopy," *Journal of Materials Science*, vol. 44, no. 21, pp. 5788–5794, 2009.

[9] D. Gastaldi, E. Boccaleri, F. Canonico, and M. Bianchi, "The use of Raman spectroscopy as a versatile characterization tool for calcium sulphoaluminate cements: a compositional and hydration study," *Journal of Materials Science*, vol. 42, no. 20, pp. 8426–8432, 2007.

[10] N. Singh and S. P. Singh, "Electrical resistivity of self consolidating concretes prepared with reused concrete aggregates and blended cements," *Journal of Building Engineering*, vol. 25, Article ID 100780, 2019.

[11] Y. Liao, X. Wei, and G. Li, "Early hydration of calcium sulfoaluminate cement through electrical resistivity measurement and microstructure investigations," *Construction and Building Materials*, vol. 25, no. 4, pp. 1572–1579, 2011.

[12] X. S. Wei and L. Z. Xiao, "Study on hydration of Portland cement using an electrical resistivity method," *Journal of the Chinese Ceramic Society*, vol. 32, no. 1, pp. 34–38, 2004.

[13] Y. S. Liao, P. F. Xu, H. M. Yang, G. S. Liao, and X. Zhong, "Hydration process of calcium aluminate cement at early age investigated by electrical resistivity method," *Journal of the Chinese Ceramic Society*, vol. 46, no. 5, pp. 657–661, 2018.

[14] F. D. Tamás, "Electrical conductivity of cement pastes," *Cement and Concrete Research*, vol. 12, no. 1, pp. 115–120, 1982.

[15] Z. Li, L. Xiao, and X. Wei, "Determination of concrete setting time using electrical resistivity measurement," *Journal of Materials in Civil Engineering*, vol. 19, no. 5, pp. 423–427, 2007.

[16] B. Dong, J. Zhang, Y. Wang, G. Fang, Y. Liu, and F. Xing, "Evolutionary trace for early hydration of cement paste using electrical resistivity method," *Construction and Building Materials*, vol. 119, pp. 16–20, 2016.

[17] P. Gu, Y. Fu, and J. J. Beaudoin, "A study of the hydration and setting behaviour of OPC-HAC pastes," *Cement and Concrete Research*, vol. 24, no. 4, pp. 682–694, 1994.

[18] W. J. Mccarter, T. M. Chrisp, G. Starrs, and J. Blewett, "Characterization and monitoring of cement-based systems using intrinsic electrical property measurements," *Cement and Concrete Research*, vol. 33, no. 2, pp. 197–206, 2003.

[19] T. B. Sui, X. H. Zeng, Y. J. Xie et al., "Early age cement hydration behavior by resistivity method," *Journal of the Chinese Ceramic Society*, vol. 36, no. 4, pp. 431–435, 2008.

[20] Z. Y. Liu, Y. S. Zhang, G. W. Sun, Q. Jiang, and W. H. Zhang, "Resistivity method for monitoring the early age pore structure evolution of cement paste," *Journal of Civil, Architectural and Environmental Engineering*, vol. 34, no. 5, pp. 148–153, 2012.

[21] J. S. Qian, L. Zhang, X. W. Jia, and Y. D. Dang, "Progress and prospect of testing method based on electric field in evaluation concrete permeability," *Materials Review*, vol. 25, no. 21, pp. 124–128, 2011.

[22] A. A. Kyi and B. Batchelor, "An electrical conductivity method for measuring the effects of additives on effective diffusivities in Portland cement pastes," *Cement and Concrete Research*, vol. 24, no. 4, pp. 752–764, 1994.

[23] ASTM C1202, *Standard Test Method for Electrical Indication of Concrete's Ability to Resist Chloride Ion Penetration*, ASTM International, West Conshohocken, PA, USA, 2007.

[24] L. Z. Xiao, Z. Ren, W. C. Shi, and X. S. Wei, "Experimental study on chloride permeability in concrete by non-contact electrical resistivity measurement and RCM," *Construction and Building Materials*, vol. 123, pp. 27–34, 2018.

[25] X. Wei, L. Xiao, and Z. Li, "Prediction of standard compressive strength of cement by the electrical resistivity measurement," *Construction and Building Materials*, vol. 31, pp. 341–346, 2012.

[26] N. Singh and S. P. Singh, "Evaluating the performance of self compacting concretes made with recycled coarse and fine aggregates using non destructive testing techniques," *Construction and Building Materials*, vol. 181, pp. 73–84, 2018.

[27] K. Hornbostel, C. K. Larsen, and M. R. Geiker, "Relationship between concrete resistivity and corrosion rate-a literature review," *Cement and Concrete Composites*, vol. 39, pp. 60–72, 2013.

[28] R. A. Medeiros-Junior and M. G. Lima, "Electrical resistivity of unsaturated concrete using different types of cement," *Construction and Building Materials*, vol. 107, pp. 11–16, 2016.

[29] S. E. S. Mendes, R. L. N. Oliveira, C. Cremonez, E. Pereira, E. Pereira, and R. A. Medeiros-Junior, "Electrical resistivity as a durability parameter for concrete design: experimental data versus estimation by mathematical model," *Construction and Building Materials*, vol. 192, pp. 610–620, 2018.

[30] P. M. Wang, N. Li, L. L. Xu, and G. F. Zhang, "Hydration characteristics and strength development of sulphoaluminate cement cured at low temperature," *Journal of the Chinese Ceramic Society*, vol. 45, no. 2, pp. 242–248, 2017.

[31] Z. Xu, W. L. Zhou, and M. Deng, "Stability of hardened sulphaluminate cement paste treated at high temperature," *Journal of the Chinese Ceramic Society*, vol. 29, no. 2, pp. 104–108, 2001.

[32] H. F. W. Taylor, *Cement Chemistry*, Thomas Telford Publishing, London, UK, 2nd edition, 1997.

[33] L. L. Xu, X. J. Yang, P. M. Wang, and K. Wu, "Influences of curing temperature on the microstructure evolution of calcium sulfoaluminate cement based on ternary blends," *Journal of Building Materials*, vol. 19, no. 6, pp. 983–998, 2016.

[34] L. Pelletier-chaignat, F. Winnefeld, B. Lothenbach, and C. J. Müller, "Beneficial use of limestone filler with calcium sulphoaluminate cement," *Construction and Building Materials*, vol. 26, no. 1, pp. 619–627, 2012.

[35] L. Xu, S. Liu, N. Li, Y. Peng, K. Wu, and P. Wang, "Retardation effect of elevated temperature on the setting of calcium sulfoaluminate cement clinker," *Construction and Building Materials*, vol. 178, pp. 112–119, 2018.

[36] P. Wang, N. Li, and L. Xu, "Hydration evolution and compressive strength of calcium sulphoaluminate cement constantly cured over the temperature range of 0 to 80°C," *Cement and Concrete Research*, vol. 100, pp. 203–213, 2017.

[37] R. B. Perkins and C. D. Palmer, "Solubility of ettringite (Ca6 [Al(OH)6]2(SO_4)3•26H2O) at 5–75°C," *Geochimica et Cosmochimica Acta*, vol. 63, no. 13/14, pp. 1969–1980, 1999.

[38] J. Chang, Y. Y. Zhang, X. P. Shang, J. Y. Zhao, and X. Yu, "Effect of AH3 phase content and hydration degree on the strength of calcium sulfoaluminate cement," *Journal of Building Materials*, vol. 19, no. 6, pp. 1028–1032, 2016.

[39] K. Kaiser and G. Guggenberger, "Mineral surfaces and soil organic matter," *European Journal of Soil Science*, vol. 54, no. 2, pp. 219–236, 2003.

[40] L. Li, R. Wang, and S. Zhang, "Effect of curing temperature and relative humidity on the hydrates and porosity of calcium sulfoaluminate cement," *Construction and Building Materials*, vol. 213, pp. 627–636, 2019.

[41] B. Lothenbach, F. Winnefeld, C. Alder, E. Wieland, and P. Lunk, "Effect of temperature on the pore solution, microstructure and hydration products of Portland cement pastes," *Cement and Concrete Research*, vol. 37, no. 4, pp. 483–491, 2007.

[42] S. A. Abo-El-Enein, F. I. El-Hosiny, S. M. A. El-Gamal, M. S. Amin, and M. Ramadan, "Gamma radiation shielding, fire resistance and physicochemical characteristics of Portland cement pastes modified with synthesized Fe_2O_3 and ZnO nanoparticles," *Construction and Building Materials*, vol. 173, pp. 687–706, 2018.

[43] Z. W. Wu, "An approach to the recent trends of concrete science and technology," *Journal of the Chinese Ceramic Society*, vol. 7, no. 3, pp. 262–270, 1979.

[44] T. C. Powers, "A working hypothesis for further studies of frost resistance of concrete," *ACI Journal Proceedings*, vol. 41, no. 1, pp. 245–272, 1945.

[45] X. F. Li, *Anti-Frost Design Method and Preventive Measures for Concrete Structure in the Qinghai-Tibet Plateau (Dissertation)*, Southeast University, Nanjing, China, 2015.

[46] Q. Li, S. Xu, and Q. Zeng, "The effect of water saturation degree on the electrical properties of cement-based porous material," *Cement and Concrete Composites*, vol. 70, pp. 35–47, 2016.

[47] L. L. Xu, S. H. Fan, G. F. Zhang, and P. M. Wang, "Temperature sensitivity of hydration properties of calcium sulfoaluminate cement based blends," *Journal of the Chinese Ceramic Society*, vol. 45, no. 11, pp. 1613–1620, 2017.

[48] L. Arnaut, S. Formosinho, and H. Burrows, *Chemical Kinetics: From Molecular Structure to Chemical Reactivity*, Elsevier Science, Amsterdam, Netherland, 2007.
[49] Z. A. Zhu and W. J. Ruan, *Physical Chemistry*, Science Press, Beijing, China, 2018.